Detection of Target Distance in the Presence of an Interfering Reflection Using a Frequency-Stepped Double Side-Band Suppressed Carrier Microwave Radar System

Gary A. Ybarra, *Student Member, IEEE*, Sasan H. Ardalan, *Member, IEEE*, Chase P. Hearn, Robert E. Marshall, and Robert T. Neece, *Member, IEEE*

Abstract—**A technique for detecting the distance to a highly reflective target in the presence of an interfering reflection using a frequency-stepped double side-band suppressed carrier (DSBSC) microwave–millimeter-wave radar system is analytically derived. Although this system is being developed for measuring nonuniform electron plasma densities as a function of distance from a heat tile on a space reentry vehicle, the technique is quite general and could be applied to other short-range radar problems. The main result of the analysis shows that the measured group delays produced by the DSBSC system possess a periodicity inversely proportional to the difference between the time delays to the target and interferer, independent of the signal-to-interference ratio (SIR). Thus, if the distance to the interferer is known, then the periodicity of the measured group delays may be used to extract the target distance, independent of SIR. Simulation results are presented in the context of electron plasma density range estimation using a block diagram communications CAD tool. A unique and accurate plasma model is introduced. A high-resolution spectral estimation technique based on an autoregressive time series analysis is applied to the measured group delays, and it is shown that accurate target distance estimates may be obtained, independent of SIR.**

I. Introduction

CONVENTIONAL pulsed radar has a range resolution which is inversely proportional to the bandwidth of the transmitted pulse [1]. Thus, applications requiring detection of extremely small changes in target position must employ very high bandwidth pulses if the conventional pulsed technique is used. The application of radar distance measurement examined in this paper is to determine the nonuniform electron plasma density profile which is created at distances from 0 to 15 cm from the heat tile of a space reentry vehicle. The accuracy requirement is ± 0.5 cm. The first implementation of this system is scheduled for deployment in a 1995 NASA shuttle mission. Electromagnetic energy launched into a nonuniform plasma, depending on the frequency, penetrates to different depths and is then reflected. The energy of a wide-bandwidth pulse would be smeared owing to the ambiguity in the location of the plasma reflection. Thus, conventional pulsed radar is unacceptable for this application, and an alternative distance measurement scheme is required.

This paper presents an analytical derivation of a new technique for detecting the distance to a highly reflective target in the presence of an interfering reflection using a frequency-stepped double side-band suppressed carrier (DSBSC) microwave–millimeter-wave radar system. The stepped DSBSC system transmits microwave energy at two distinct, narrowly spaced frequencies centered on the suppressed carrier. The receiver then measures the difference between the phases of the two sinusoidal echoes which result from the combined reflections of the target and interferer. This phase difference is then used to approximate the slope of the propagation path phase response, yielding a group delay estimate. This process was examined in [2] and termed AM CW radar. It was recognized that the simple AM CW process produced erroneous distance estimates unless the echo from the primary target was much stronger than the echo from the interferer. It is because of this requirement that the AM approach has received little attention [2]. Our approach extends the technique of AM CW radar such that the accuracy of the target distance estimate is independent of the relative strengths of the primary and interfering echoes. The carrier is stepped through a sequence of N discrete frequencies and the receiver acquires a set of N group delay estimates. A previously reported technique for detecting the target distance using a stepped DSBSC

Manuscript received August 7, 1990; revised December 10, 1990. This work was supported in part by the National Aeronautics and Space Administration Langley Research Center under Contract NAS1-18925.

G. A. Ybarra and S. H. Ardalan are with the Department of Electrical and Computer Engineering, North Carolina State University, Box 7911, Raleigh, NC 27695.

C. P. Hearn and R. T. Neece are with the NASA Langley Research Center, Hampton, VA 23665.

R. E. Marshall is with the Research Triangle Institute, Research Triangle Park, NC 27709.

IEEE Log Number 9143468.

0018-9480/91/0500-0809$01.00 ©1991 IEEE

approach [3] averages the N group delay estimates in order to obtain an estimate of the target distance. This averaging approach was found to provide an accurate target distance estimate provided the echo from the target is larger than the echo from the interferer. When the echo from the interferer is greater than the echo from the target, the averaging technique is known to fail. This paper analytically proves that the average group delay is the propagation time delay to the target when the signal to interference ratio (SIR) is greater than 0 dB, and is the propagation time delay to the interferer when the SIR is less than 0 dB, thus providing a mathematical basis for the previously reported measurements. However, the main result of the analysis shows that the measured group delays possess a periodicity inversely proportional to the difference between the time delays to the target and interferer, *independent of SIR*. Thus, if the distance to the interferer is known, then the periodicity of the measured group delays may be used to extract the target distance, independent of SIR. Although the technique is general, simulation results are presented for measuring nonuniform electron plasma density as a function of distance. The interfering reflection is due to the high-dielectric-constant reaction cured glass (RCG) coating on a heat tile. These simulations are performed using a block diagram communications system CAD tool employing a unique and accurate plasma model. A high-resolution spectral estimation technique based on an autoregressive time series analysis is applied to the measured group delays, and it is shown that accurate target distance estimates may be obtained, independent of SIR.

Other short-range radar techniques have been proposed such as the diplex Doppler method [4] and a sinusoidal FM method [5]. In the diplex Doppler method, the transmitter is time-shared between two closely spaced frequencies. The phase difference between the two slightly displaced Dopplers at the receiver depends on the range to the target. However, since the range is extracted from the phase difference in the Doppler signal, no information is obtained without significant target velocity. The sinusoidal FM technique extracts the target range from the relative phase of the received signal, which does not depend on target speed. Unfortunately, the sinusoidal FM system is relatively complex to implement [5]. The advantage of our technique is that it is simple to implement, requiring minimal hardware and space, and provides accurate target distance estimates. An important additional advantage of the frequency-stepped DSBSC system over other techniques such as a stepped-carrier technique that generates an impulse response and uses range-gating to separate the target from the interferer is its immunity to Doppler shift due to target motion. The relative Doppler immunity of the frequency-stepped DSBSC technique is due to the fact that the effective Doppler shift is at twice the modulation frequency, which is much smaller than the microwave carrier.

This paper is organized as follows. First, the plasma density measurement environment is described in detail.

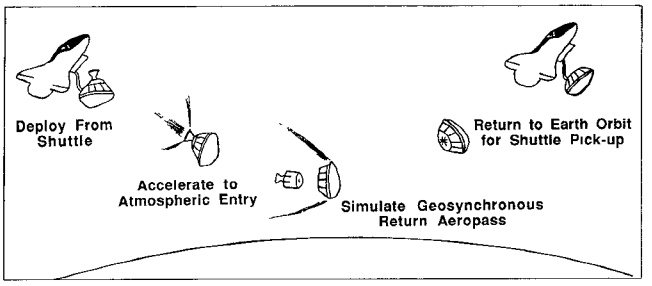

Fig. 1. The NASA Aeroassist Flight Experiment (AFE).

Then, the frequency-stepped DSBSC technique is derived and its properties illustrated. Finally, simulation results are presented which provide an illustrative example of the technique. This is followed by some concluding remarks.

II. Plasma Density Measurement Environment

The electron plasma density measurements will take place as part of the NASA Aeroassist Flight Experiment (AFE), which is illustrated in Fig. 1. The shuttle will deploy the AFE vehicle, which will then be accelerated to atmospheric entry velocity. During the 600 s aeropass, the high temperature in the proximity of the nonablating heat tiles will generate a dynamic plasma. The friction created will slow the craft, providing an aerobrake. Following the aeropass, the AFE vehicle will attain a low earth orbit to be retrieved by the shuttle. One purpose of this experiment is to ascertain the feasibility of using the atmosphere as an aerobrake, which requires accurate measurement of the plasma density profile. The plasma profile data will be used to confirm or improve the flow field predictions made by computational fluid dynamics. The system which will perform the plasma density measurements is called the microwave reflectometer ionization sensor (MRIS). The MRIS antennas will be mounted behind the stagnation region tiles, where the plasma flow field is laminar. Polarization is not an issue because the plasma density is expected to be constant in the transverse plane.

There exist several predictions of the plasma density profiles that are to be measured. One such prediction is based on computational fluid dynamics (CFD) and is considered to be one of the better predictions presently available. An example of a CFD predicted profile is shown in Fig. 2. The distance values shown are referenced to the outer surface of the heat tiles of the AFE vehicle. Distances referenced from the heat tiles are referred to as *standoff* distances.

Electron plasma may be characterized by its relative dielectric constant [6], given by

$$\epsilon_r = 1 - \frac{q^2 N}{m\epsilon_0 \omega^2 \left(1 - j\frac{\nu}{\omega}\right)} \tag{1}$$

where q is the electron charge, N is the electron density, m is the electron mass, ϵ_0 is the permittivity of free space,

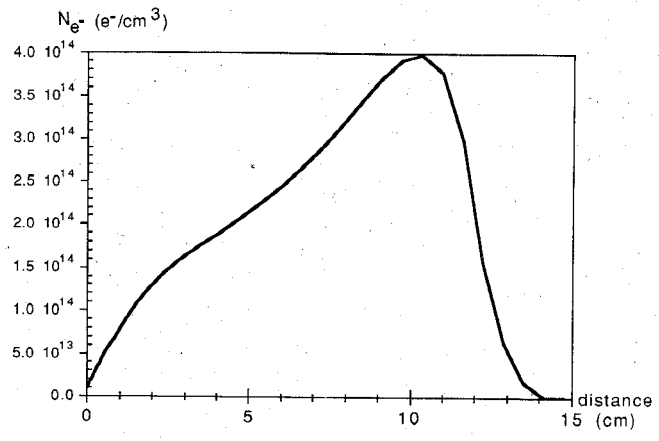

Fig. 2. Computational fluid dynamics (CFD) prediction of the electron density profile at 87 km altitude.

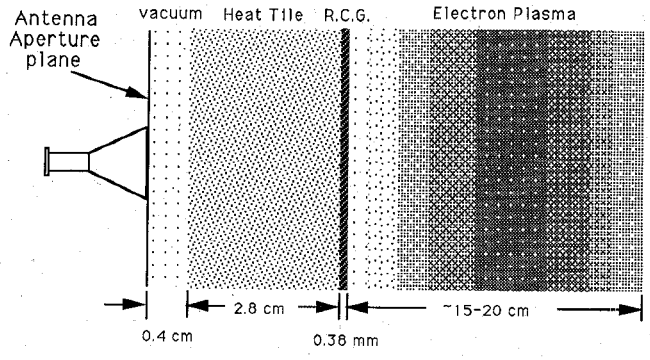

Fig. 3. Microwave reflectometer ionization sensor (MRIS) propagation path.

ω is the angular frequency of propagating electromagnetic (EM) energy, and ν is the plasma collision frequency. Considering EM frequencies much greater than ν, and substituting the values for the constants, (1) may be approximated well by

$$\epsilon_r = 1 - \frac{81N}{f^2} \tag{2}$$

where the EM frequency, f, is in kHz, and the electron density, N, is in e^-/cm^3. Unlike other materials, the group velocity, v_g, of EM energy in a plasma is the free-space velocity, c, scaled by $\sqrt{\epsilon_r}$:

$$v_g = c\sqrt{\epsilon_r} = c\sqrt{1 - \frac{81N}{f^2}}\ . \tag{3}$$

There exists a critical frequency, f_{cr}, for a given electron density, which occurs when $\epsilon_r = 0$. At this point in the plasma, called the turning point, the plasma becomes a perfect reflector. That is, at the turning point, the reflection coefficient becomes $\rho = -1$, and interestingly the group velocity goes to zero. For frequencies much greater than f_{cr}, $\epsilon_r \approx 1$ and the plasma behaves similar to free space. For frequencies less than f_{cr}, $\epsilon_r < 0$ and the plasma behaves like a waveguide below its cutoff frequency. That is, only evanescent modes are present and no propagation occurs. As an example of a plasma density distance measurement, consider the CFD profile in Fig. 2. Suppose an EM wave is launched at a frequency of 140 GHz. The critical density, N_c, at this frequency may be calculated from (2) to be $2.42 \cdot 10^{14}$ e^-/cm^3 and is located at a standoff distance of 6 cm. The EM wave will penetrate into the plasma until it is reflected at the turning point and returns as an echo. If the round-trip travel time is measured and an average velocity of propagation is assumed, then an estimate of the standoff distance can be made. Although this technique is impractical because of the extremely small time interval, it serves to illustrate the plasma density measurement concept. The velocity of energy propagation in the plasma varies with the electron density profile according to (3). However, if the electron density variation is linear with distance, then the average velocity is well approximated by the convenient value $c/2$. The CFD predicted profile shown in Fig. 2 is not exactly linear, but it is close enough to warrant the use of $c/2$ as a first approximation to the average velocity.

It has been predicted that electron densities in the range of 10^{12}–10^{15} e^-/cm^3 are expected to be encountered in the measurement range of 0–15 cm from the heat tile during the aeropass. In order to measure this electron density range, frequencies of 9–284 GHz would be required. Owing to the MRIS system space and weight constraints, as well as practical microwave and millimeter-wave sources, four center frequencies have been selected: 20, 44, 95, and 140 GHz. Thus, only four densities will be measured. Measurement of these four densities will be performed sequentially and repeated continuously for the first 500 s of the aeropass and therefore can be tracked as a function of time. This information should provide enough data to approximate well the electron density profile as a function of time.

In order to launch an EM wave into the plasma, an antenna is mounted behind the heat tiles of the AFE vehicle. The propagation path is illustrated in Fig. 3. The heat tile has a dielectric constant $\epsilon_r = 1.36$. Thus, a small dielectric discontinuity occurs at the vacuum–tile interface which will cause a small strength spurious reflection. However, there is a thin RCG coating on the outer surface of the heat tile whose dielectric constant ϵ_r is 4.8. Therefore, a significant spurious reflection will occur at the tile–RCG interface. This reflection is considered interference and represents a potentially significant obstacle for the plasma density measurement. It will be shown, however, that our measurement technique is not only immune to the interfering reflection, but utilizes the prior knowledge of its location as a reference, leading to accurate plasma density position measurements.

III. Analytical Derivation of the DSBSC Distance Measurement Technique

The DSBSC distance measurement technique is based on the relationship between the phase response and time delay of a linear system. For a linear system, the time

delay is the negative slope of the system phase response and is therefore, in general, a function of frequency:

$$t_d = -\frac{d\theta(\omega)}{d\omega}. \tag{4}$$

In the time domain, the simplest realistic model for the impulse response of a propagation channel known to contain an interfering reflector and a highly reflective target is given by

$$h(t) = A_p\delta(t - t_{dp}) + A_t\delta(t - t_{dt}) \tag{5}$$

where $\delta(t)$ is the Dirac delta function, and t_{dp} and t_{dt} are the round-trip time delays to the primary target and interfering reflector respectively. The constants A_p and A_t represent the combination of path loss and reflection coefficient associated with each reflector. This model assumes that a transmitted microwave energy burst will return primarily as two temporally concentrated pulses. Simulation results will show that the consequence being derived here using this assumption is accurate for the plasma measurement application.

The frequency response associated with a channel whose impulse response is given by (5) is

$$H(f) = A_p e^{-j\omega t_{dp}} + A_t e^{-j\omega t_{dt}} \tag{6}$$

where $\omega = 2\pi f$. Separating $H(f)$ into its real and imaginary parts yields

$$H(f) = A_p\cos(\omega t_{dp}) + A_t\cos(\omega t_{dt}) - j\left[A_p\sin(\omega t_{dp}) + A_t\sin(\omega t_{dt})\right]. \tag{7}$$

The phase of this frequency response function is

$$\theta(f) = \tan^{-1}\left(\frac{-\left(A_p\sin(\omega t_{dp}) + A_t\sin(\omega t_{dt})\right)}{A_p\cos(\omega t_{dp}) + A_t\cos(\omega t_{dt})}\right). \tag{8a}$$

The phase response may be expressed in the alternative form

$$\theta(f) = -2\pi f t_{dp} + \tan^{-1}\left(\frac{A_t\sin\left(2\pi f(t_{dp} - t_{dt})\right)}{A_p + A_t\cos\left(2\pi f(t_{dp} - t_{dt})\right)}\right). \tag{8b}$$

The negative derivative of the phase response (8a) with respect to angular frequency ω is the channel time delay and is given by

$$t_d = \frac{\beta}{1 + \left(\dfrac{A_p\sin(\omega t_{dp}) + A_t\sin(\omega t_{dt})}{A_p\cos(\omega t_{dp}) + A_t\cos(\omega t_{dt})}\right)^2} \tag{9}$$

where

$$\beta = \frac{\left[A_p\cos(\omega t_{dp}) + A_t\cos(\omega t_{dt})\right]\left[A_p t_{dp}\cos(\omega t_{dp}) + A_t t_{dt}\cos(\omega t_{dt})\right] + \left[A_p\sin(\omega t_{dp}) + A_t\sin(\omega t_{dt})\right]\left[A_p t_{dp}\sin(\omega t_{dp}) + A_t t_{dt}\sin(\omega t_{dt})\right]}{\left[A_p\cos(\omega t_{dp}) + A_t\cos(\omega t_{dt})\right]^2} \tag{10}$$

Using the definition

$$\alpha = \frac{A_p}{A_t} \tag{11}$$

which is the SIR, and elementary trigonometric identities, the above expression for the channel time delay may be simplified to

$$t_d = \frac{\alpha^2 t_{dp} + t_{dt} + \alpha(t_{dp} + t_{dt})\cos\left(2\pi f(t_{dp} - t_{dt})\right)}{1 + \alpha^2 + 2\alpha\cos\left(2\pi f(t_{dp} - t_{dt})\right)}. \tag{12}$$

This function is periodic in frequency with period

$$T_f = \frac{1}{t_{dp} - t_{dt}}. \tag{13}$$

Thus, one mechanism for determining the distance to the primary target is to estimate the period of the group delay measurement. Since the time delay to the interfering RCG coating, t_{di}, is known in advance, the period (13) of the measured group delay yields the delay time to the plasma turning point t_{dp}. Using an estimate of the average energy propagation velocity for the plasma allows t_{dp} to be converted into a distance measurement. It will be shown through simulation that this method of extracting the turning point location may lead to accurate range estimates.

A previously reported method of extracting the turning point standoff distance using the frequency-stepped DSBSC approach [3] is to average the phase measurements or, equivalently, the time delay measurements. The average time delay may be derived analytically by integrating the time delay expression (12) over one period and dividing the result by the period. The expression for the time delay (12) has the form

$$f(x) = \frac{a + b\cos(x)}{c + d\cos(x)} \tag{14}$$

where the following substitutions have been made:

$$a = \alpha^2 t_{dp} + t_{dt} \qquad b = \alpha(t_{dp} + t_{dt}) \qquad c = 1 + \alpha^2$$
$$d = 2\alpha \qquad x = 2\pi f(t_{dp} - t_{di}).$$

Given the fact that $c^2 \geqslant d^2$ for all α, the integral of $f(x)$ over one period is

$$\int_{-\pi}^{\pi}\frac{a + b\cos(x)}{c + d\cos(x)}\,dx = \left[\frac{bx}{d} + \frac{2\left(a - \dfrac{bc}{d}\right)}{\sqrt{c^2 - d^2}}\tan^{-1}\left(\frac{\sqrt{c^2 - d^2}\tan\left(\dfrac{x}{2}\right)}{c + d}\right)\right]_{-\pi}^{\pi} \tag{15}$$

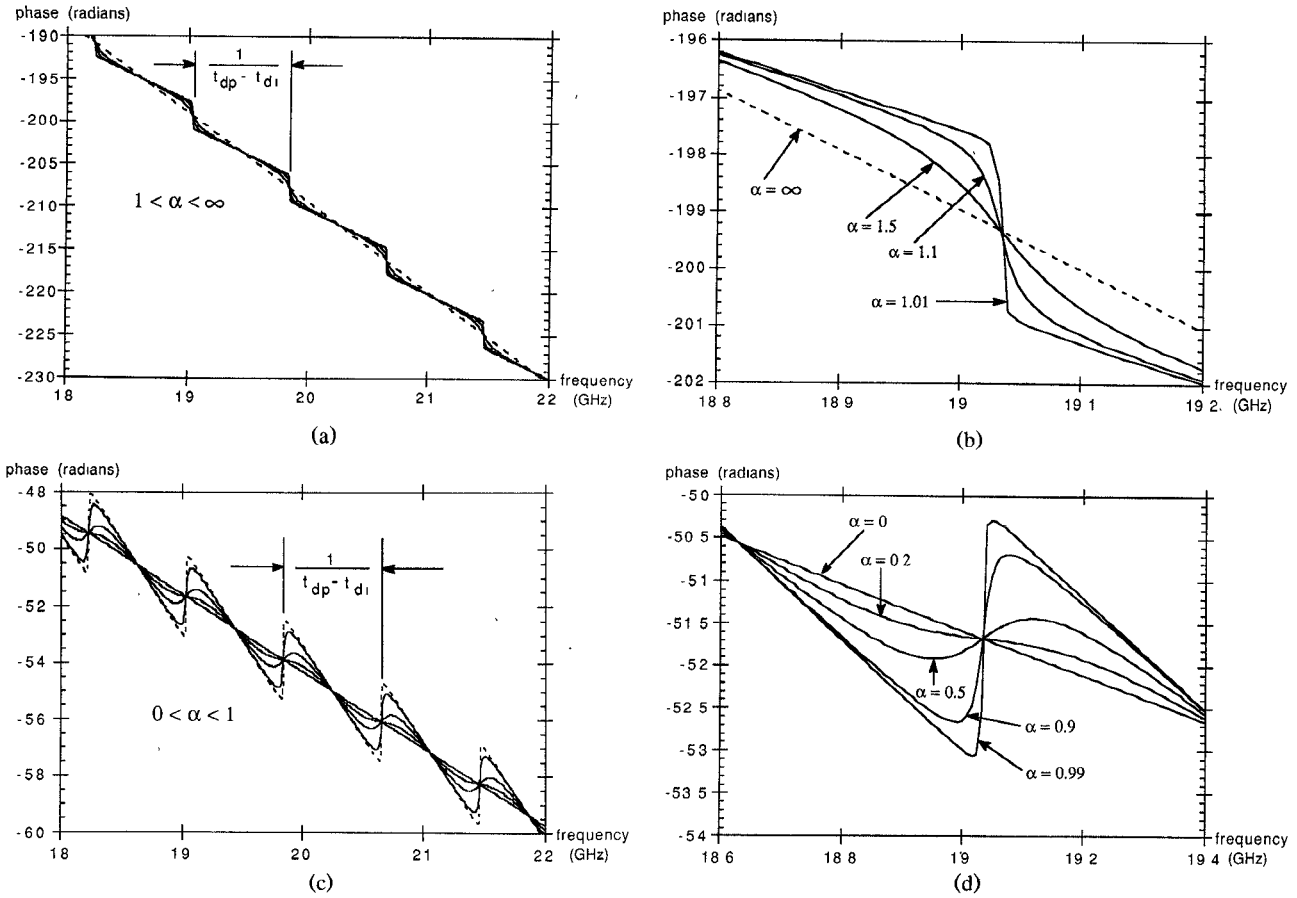

Fig. 4. (a) Theoretical frequency-stepped DSBSC phase measurement assuming two scatterers and SIR > 1. (b) Theoretical frequency-stepped DSBSC phase measurement assuming two scatters and SIR > 1 (zoomed view). (c) Theoretical frequency-stepped DSBSC phase measurement assuming two scatterers and SIR < 1. (d) Theoretical frequency-stepped DSBSC phase measurement assuming two scatterers and SIR < 1 (zoomed view).

The antiderivative is easily verified by differentiation. Evaluation of (15) and dividing by the period 2π yields the average value, f_{av}, given by

$$f_{av} = \frac{1}{2\pi}\int_{-\pi}^{\pi} f(x)\,dx = \frac{b}{d} + \frac{a - \dfrac{bc}{d}}{\sqrt{c^2 - d^2}}. \tag{16}$$

Now resubstituting the coefficients a, b, c, and d yields the average time delay, $t_{d\,av}$, given by

$$t_{d\,av} = \frac{t_{dp} + t_{di}}{2} + \frac{\alpha^2 t_{dp} + t_{di} - \dfrac{(t_{dp} + t_{di})(1+\alpha^2)}{2}}{|\alpha^2 - 1|}. \tag{17}$$

This expression may now be simplified to yield the result

$$t_{d\,av} = \frac{1}{2}\left(t_{dp} + t_{di} + \frac{\alpha^2 - 1}{|\alpha^2 - 1|}(t_{dp} - t_{di})\right) \tag{18}$$

which may be further simplified to obtain the following final result:

$$t_{d\,av} = t_{dp}, \qquad \alpha > 1,$$
$$t_{d\,av} = t_{di}, \qquad \alpha < 1.$$

The result for the special case of $\alpha = 1$ may be obtained by applying L'Hospital's rule to (18), which yields

$$t_{d\,av} = \frac{t_{dp} + t_{di}}{2}. \tag{19}$$

The analytical results derived here for the time delay obtained using the DSBSC technique may be interpreted as follows. If the plasma reflection is stronger than the reflection from the interfering RCG ($\alpha > 1$) and if an accurate technique for extracting the average phase is employed, then the turning point may be established. If the SIR is less than 1 ($\alpha < 1$) and phase averaging is employed, an erroneous estimate of the turning point will result. It has been analytically shown, however, that an accurate estimation of the turning point may be extracted from the phase measurements using the relation between the group delay period (13) and the time delay difference, $t_{dp} - t_{di}$, regardless of the signal-to-interference ratio. This result shows the potential immunity of the DSBSC technique to a weak primary target reflection.

The theoretical phase measurement assuming two scatterers has been shown to be

$$\theta(f) = \tan^{-1}\left(\frac{-\left(A_p \sin(\omega t_{dp}) + A_i \sin(\omega t_{di})\right)}{A_p \cos(\omega t_{dp}) + A_i \cos(\omega t_{di})}\right). \tag{8a}$$

Plots of the theoretical phase (8a) over a 4 GHz bandwidth, beginning at 18 GHz, for various SIR's are shown in parts (a)–(d) of Fig. 4 for the two-scatterer idealization of the propagation path of Fig. 3 with the plasma critical density at 9 cm for 20 GHz (an average group velocity of $c/2$ has been assumed for the plasma). Several important observations can be made from these graphs. First of all, parts (a) and (b) of Fig. 4 show that if the interferer is absent, the SIR $\alpha = \infty$, and the phase is linear owing purely to the primary target reflection. As the SIR deteriorates, approaching unity from above, an oscillation about this linear phase occurs with increasing amplitude and may be seen most clearly in Fig. 4(b) which is a zoomed view of Fig. 4(a). However, the periodicity of this oscillation does not change with SIR except in the extreme case $\alpha = \infty$. Parts (c) and (d) of the figure illustrate a similar phenomenon for cases of SIR's between 0 and 1. When $\alpha = 0$, the phase becomes linear once again, and this is due purely to the interfering RCG. Note that the periodicity of the oscillations, once again, does not vary with SIR. When the SIR is identically equal to 1, the phase function will converge to a linear phase with an intermediate slope exactly half way between the extreme cases of $\alpha = 0$ and $\alpha = 1$, exactly as predicted by the theory developed earlier. It has been shown analytically that the oscillation about the linear case has a period which is the inverse of the difference in time delays to each scatterer. This relation is indicated in parts (a) and (c) of Fig. 4, and special note should be made that this period is constant, independent of SIR.

The time delay may be calculated from the phase response by differentiating with respect to ω and then may be converted into a distance measurement as a function of frequency using an average plasma velocity. Using an average plasma velocity of $c/2$, several theoretical distance measurements using the same 4 GHz bandwidth as was used in (a)–(d) of Fig. 4 are shown in Fig. 5 for various SIR's. It has been proved that if the SIR is greater than 1, then the average value of the distance function for any SIR is the primary target distance. Furthermore, it has been proved that if the SIR is less than 1, then the distance function has an average value equal to the distance to the interfering RCG. Averages were taken for each of the distance functions shown in Fig. 5. When the SIR is such that the deviation from the mean value is small (α near ∞ or α near 0), then only a few points need to be averaged in order to obtain an accurate estimate of the average. However, when the SIR approaches unity from above or below, many points are required for an accurate estimate of the average. This is due to the near cusps that develop at the function extrema. The periodicity is shown to contain the standoff distance information, as expected from the theoretical derivation. An important point must be made regarding the process of averaging the distance measurements. Accurate estimates require that an integral number of half periods be averaged or that a large number of half periods be averaged. When the target and interferer are far apart, several periods are present. When the target is near the interferer, the period approaches zero, which may cause an inaccurate distance measurement using the distance averaging approach, especially if the SIR is near unity and only a relatively small number of measurements are averaged. In this case, it is fortunate that the distance information may still be extracted from the periodicity of the phase measurements, even when the oscillation is weak.

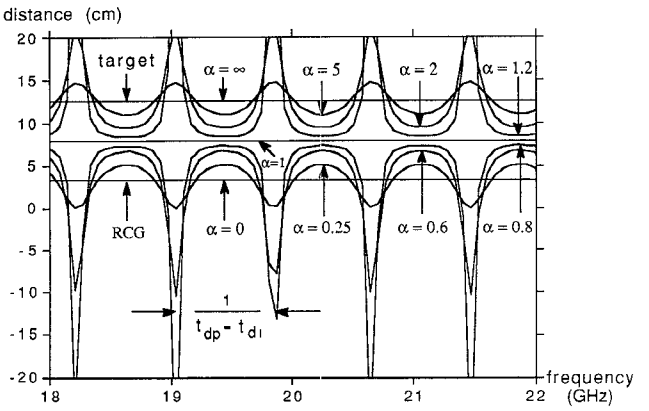

Fig. 5. Theoretical distance measurements as a function of frequency for the frequency-stepped DSBSC system.

It still remains to be shown whether the two-scatterer theory developed earlier is applicable to the much more complex vacuum/tile/RCG/plasma propagation path. Simulation results will now be presented which show that the theory is indeed applicable.

IV. Plasma Density Measurement Using the Frequency-Stepped DSBSC Technique

The frequency-stepped DSBSC system simultaneously transmits two sinusoids centered on the suppressed carrier. The differential phase shift between these two side bands induced by the propagation channel is then measured at the receiver, producing an incremental estimate of the slope of the phase response. This estimate of the phase response slope is the estimated group delay. A measurement is made at N discrete frequencies, spanning a total bandwidth of $N\Delta f$, where Δf is the frequency step size. An implementation of the DSBSC system is shown in Fig. 6. The transmitter consists of an upper single side band frequency-stepped carrier generator whose output is modulated by another sinusoid of frequency f_M. The received echo is passed through a square-law device and band-pass filtered to extract the component at frequency $2f_M$ produced by the square-law device since it is this tone that contains the phase differential $\theta_2 - \theta_1$, where θ_2 and θ_1 are the channel-induced phase shifts of the upper and lower side bands respectively. This signal is then simultaneously mixed with an in-phase and quadrature sinusoid at frequency $2f_M$, phase coherent with the modulator in the transmitter. After low-pass filtering, the result is a pair of quadrature signals from which the phase differential $\theta_2 - \theta_1$ may be extracted via a four-quadrant arctangent operation. The round-trip

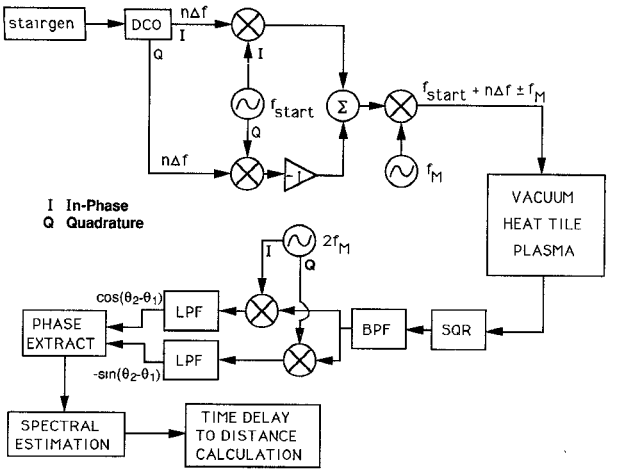

Fig. 6. Block diagram of the frequency-stepped DSBSC distance measurement system.

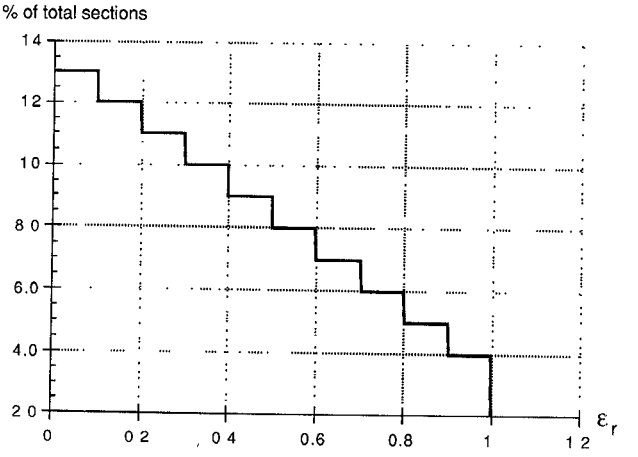

Fig. 7. Dynamic allocation of plasma model slab widths.

group delay estimate, t_d, is obtained from the phase difference by

$$t_d = -\frac{d\theta(\omega)}{d\omega} \approx -\frac{\theta_2-\theta_1}{\omega_2-\omega_1} = -\frac{\theta_2-\theta_1}{4\pi f_M}. \quad (20)$$

The maximum unambiguous range corresponds to a 2π variation in $\theta_2-\theta_1$ and is given by

$$R_{\max} = \frac{1}{2} v_g t_d = \frac{c}{8f_M} \quad (21)$$

using an average plasma velocity of $c/2$. Since it is desired to measure electron densities with standoff distances from 0 to 15 cm, we chose to use $f_M = 125$ MHz in our simulations, which provides a maximum unambiguous range of approximately 30 cm from the antenna aperture. The range equation (21) dictates an upper bound on f_M. The smaller the value of f_M, the better the differential phase approximates the true slope. However, as the value of f_M is reduced, the phase differential corresponding to a particular standoff distance decreases. Therefore it becomes increasingly difficult to resolve small standoff distances as f_M is decreased.

The block diagram of the DSBSC system presented in Fig. 6 shows the system exactly as implemented using CAPSIM, a hierarchical block diagram communication and signal processing simulation environment. The block "stairgen" creates a sequence of samples with a staircase amplitude which drives the digitally controlled oscillator, DCO, to produce the discrete frequency sweep of N steps over a bandwidth of $N\Delta f$. The block in Fig. 6 labeled VACUUM, HEAT TILE, PLASMA contains a unique and accurate plasma model we developed called PROPMOD. PROPMOD is, in general, a program for computer modeling and simulation of plane wave propagation in inhomogeneous media. The program uses recursive techniques to solve the boundary value problem for the electric and magnetic fields at each of the slab interfaces. The propagation path shown in Fig. 3 is modeled as a cascade of slabs of material, each having a specified set of material parameters ϵ, μ, and σ and a thickness ΔL. For example, the heat tile is specified by $\epsilon = 1.36\epsilon_0$, $\mu = \mu_0$, $\sigma = 0$, and $\Delta L = 2.8$ cm. The interesting specification is for the inhomogeneous plasma. Several applications have seen the use of homogeneous slabs in order to model inhomogeneous media. Two examples are randomes whose dielectric constants vary as a consequence of a temperature gradient [7] and waveguides loaded with a tapered dielectric in order to reduce dispersion caused by phase distortion [8]. In order to model the plasma, we slice the electron density profile into slabs of varying thickness, each characterized by its complex permittivity determined by (1). It was shown in [7] that in order to minimize modeling error, a dynamic slab thickness allocation algorithm should allocate slab thickness inversely proportional to the magnitude of the derivative of the dielectric profile with respect to distance. This constraint is required to maintain smoothness in the dielectric profile of the model since the true inhomogeneous plasma has a continuous dielectric profile, and any sudden discontinuity in the dielectric will cause spurious reflections. With a plasma model, another consideration must be made. It is important that the modeling error be relatively small in the vicinity of the turning point. Therefore, considering slope and the turning point criterion, a dynamic slab width allocation algorithm was developed which considers both criteria in the allocation process. The algorithm is quite simple and is illustrated in Fig. 7. The number of sections per unit distance is increased linearly with decreasing permittivity. Only 85% of the total allocation of sections are shown in the diagram. The remaining sections are distributed between the turning point and the end of the profile. Fig. 8 shows what happens with this distribution for three differently shaped dielectric profiles. In the linear case, the slope is constant and therefore there is a linear increase in sections per distance as the turning point is approached. In the second case, the slope is near zero for nearly half the distance to the turning point and then the slope becomes increasingly

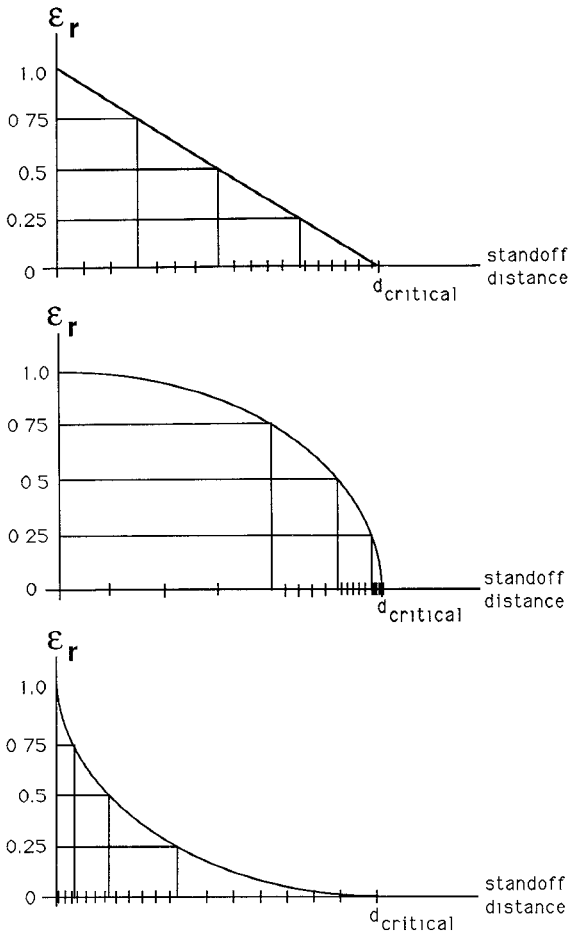

Fig. 8. Illustration of the algorithm which dynamically allocates slab thicknesses in the plasma model for various permittivity profiles. Tick spacing indicates the relative number of sections used in the plasma model.

larger (negative), causing the sections to compress nearer to the turning point. This is precisely what is desired, since the slope is steepest near the critical distance, d_c. The third case shows when a trade-off is made between slope and dielectric value. The slope is large near the front edge of the profile and approaches zero near the critical point. Thus, the algorithm allocates relatively few sections in the first few permittivity bins. However, these bins are warped into compressed standoff distance space, creating thinner slabs than would result with a linear taper. Then as the critical point is approached, the number of sections is increased with smaller dielectric, but the bins are warped into larger standoff values. Hence, a slope/turning point trade-off occurs as desired.

Now the question arises as to how many sections to use in the slab model for the plasma. For the particular CFD profile used in our simulations (Fig. 2), we found that using more than 1000 sections made very little difference in any of the phase measurements made by the DSBSC system. We chose to use 1500 sections to ensure an accurate model for all measurement cases. Using 1500 sections resulted in section sizes ranging from a few microns to a few millimeters.

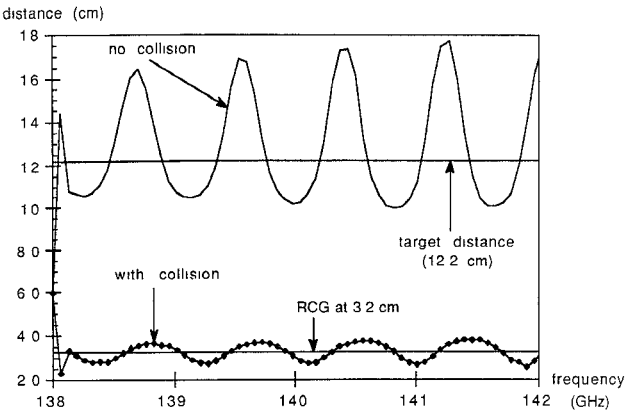

Fig. 9. Distance measurements using the frequency-stepped DSBSC system with and without loss caused by collision.

In order to illustrate the performance of the frequency-stepped DSBSC system, consider the CFD electron density profile shown in Fig. 2 scaled so that the critical density at 140 GHz is located at a standoff distance of 9 cm. Using $N = 64$ measurements with a frequency step size of $\Delta f = 64$ MHz, the DSBSC system produced the distance measurements shown in Fig. 9. When no loss from collision is included, the group delay is captured by the primary target because the reflection from the plasma is stronger than the reflection from the RCG interferer. However, when loss is included in the simulation, the reflection from the RCG is much stronger than the plasma reflection, and the group delay measurement is captured by the interfering RCG. The SIR in this case is approximately 0.1 (-20 dB). This SIR value was obtained by using a stepped CW technique and comparing the relative strengths of the plasma and interfering RCG reflections in the time domain. The averaging technique described in [3] would work if no collision were present, although it would produce an error of 0.5 cm (i.e. the average value of the no-collision case is 12.70 cm). However, the averaging technique will fail in the more realistic case which includes path loss caused by collision. Fortunately, the information containing the location of the plasma target is present in the data periodicity whether or not loss is present. It was shown in (13) that the fundamental frequency of the measurements shown in Fig. 9 is the difference in the time delays to the primary target and interferer assuming the simple two-scatterer model. There exist several ways to extract the fundamental frequency from the N data points available from a given measurement sweep. One approach would be to take an N-point discrete Fourier transform (DFT) of the data. The time resolution resulting from an N-point DFT of the frequency-stepped DSBSC distance data is

$$\Delta t = \frac{1}{2N\Delta f}. \tag{22}$$

Using an approximate average plasma group velocity of

$c/2$, the one-way distance resolution is

$$\Delta d = \frac{1}{2}\frac{c}{2}\Delta t = \frac{c}{8N\Delta f}. \quad (23)$$

Using $N = 64$ and $\Delta f = 64$ MHz, a distance resolution of $\Delta d = 0.9155$ cm results.

An alternative analysis technique is now presented for estimating the standoff distance from the periodicity of the distance measurements. It is based on autoregressive time series analysis [9], which has been applied to high resolution spectral estimation. As will be shown, time series analysis may provide a significant accuracy improvement in standoff distance estimates over that obtainable using the Fourier approach.

Consider the near periodic sequence of distance measurements shown in Fig. 9 to be approximated by the difference equation

$$d(n) = \sum_{k=1}^{3} a_k d(n-k) + u(n), \qquad n = m\Delta f, \quad 0 \leqslant m \leqslant 63 \quad (24)$$

where $d(n)$ is the sequence of distance measurements, a_k are the autoregressive coefficients, and $u(n)$ is the innovation or input driving function. Thus, $d(n)$ is being modeled as the response of a linear system whose output is the innovation plus a linear combination of the past three outputs. Such a model is called an autoregressive (AR) model of order 3. A third-order autoregressive model was chosen because a single peak in the time response is expected which requires two complex poles in the model. The other parameter is used to model deviation in the phase measurements from a pure sinusoid. In conventional time series analysis $d(n)$ would be, typically, discrete samples of a continuous-time function $d(t)$. Here, the $d(n)$ are discrete samples of a continuous-frequency function $d(f)$. If the discrete-time Fourier transform of (24) is taken, a continuous complex function of time results:

$$D(e^{j\Delta\omega t_{\text{diff}}}) = \sum_{k=1}^{3} a_k D(e^{j\Delta\omega t_{\text{diff}}}) e^{-jk\Delta\omega t_{\text{diff}}} + U(e^{j\Delta\omega t_{\text{diff}}}), \qquad \Delta\omega = 2\pi\Delta f \quad (25)$$

where $t_{\text{diff}} = t_{dp} - t_{di}$. The system time response (output D over input U) may be obtained from (25), resulting in

$$R(t_{\text{diff}}) = \frac{1}{1 - \sum_{k=1}^{3} a_k e^{-jk\Delta\omega t_{\text{diff}}}} \quad (26)$$

which is once again a complex function of time. In order to illustrate the value of this approach, the time series model (24) was applied to the collision distance data of Fig. 9. The autoregressive coefficients a_k were extracted using a conventional least-squares approach [9]. These coefficients were then substituted into (26) and the resulting squared magnitude is shown in Fig. 10. The delay estimate is 1.203 ns, as shown in the figure, and translates into a standoff estimate of 9.0225 cm, producing an error

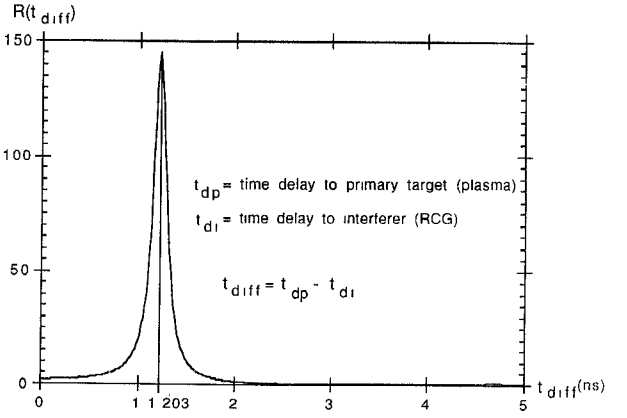

Fig. 10. Spectrum obtained from an autoregressive time series analysis of the group delay measurements made by the frequency-stepped DSBSC system.

of only 225 μm. It should be noted that (26) is a continuous function of time and does not suffer from the resolution problem which plagues the FFT approach when only a short data record is available. It is recognized that the example presented in somewhat optimistic since neither noise nor the effects of some component error contributions were included in the simulation. The simulation does include nonideal filter responses but does not incorporate the effects arising from mixer imbalances. Our plasma model accounts for reflections that occur at the vacuum–tile interface in addition to the reflections at the RCG boundaries. The intention of the example is to illuminate the fact that the technique of applying AR time series analysis to the frequency-stepped DSBSC measurements can be used to extract an accurate target distance estimate even when the SIR is significantly less than 0 dB. In our application of measuring electron plasma densities, a worst-case S/N of 30 dB is expected at the inputs to the in-phase and quadrature detectors, and S/N ratios of 50–70 dB are expected for most measurements. Hence, it is not expected that noise levels will be large enough to significantly degrade performance in the MRIS measurements. In other short-range radar problems, noise may be a significant problem and a more sophisticated spectral estimation approach such as an autoregressive moving average approach (ARMA) [9] may be required.

It has been shown that autoregressive time series analysis can be used to measure accurately the period of the distance measurements made by the DSBSC system. The example presented shows that even when the SIR is significantly less than 0 dB and the averaging technique fails as expected, the high-resolution autoregressive estimator can provide an accurate distance estimate based on the simple two-scatterer theory.

V. Conclusion

This paper has presented the derivation and analysis of a technique for measuring the distance to a highly reflective target in the presence of an interfering reflection.

The technique utilizes a frequency-stepped DSBSC system and is a candidate for use as an electron plasma density detector to be flown in the NASA Aeroassist Flight Experiment in 1995. Simulation of the system was performed using a block diagram communications system CAD tool. A unique and accurate plasma model based on plane wave propagation through slabs of inhomogeneous plane layers was introduced. A novel approach was presented for extracting the target distance from the periodicity of the measured group delays produced by the DSBSC system. The approach employed autoregressive time series analysis and was shown to provide accurate target distance estimation, even when the primary target reflection is weak compared with the interfering reflection.

Future research will be directed toward quantifying the sensitivity of this technique to multiple spurious reflections and extending the theory to account for their influence.

REFERENCES

[1] M. I. Skolnik, *Radar Handbook*. New York: McGraw-Hill, 1970.
[2] O. K. Nilssen and W. D. Boyer, "Amplitude modulated CW radar," *IRE Trans. Aerospace Navigational Electron.*, Dec. 1962.
[3] C. P. Hearn, C. R. Cockrell, and S. D. Harrah, "An analysis of the effects of spurious reflections in the MRIS distance-measurement system," NASA Technical Report, 1990.
[4] W. D. Boyer, "A diplex, Doppler phase comparison radar," in *Int. IRE Conv. Rec.*, 1962.
[5] D. M. Grimes and T. O. Jones, "Automotive radar, A brief review," *Proc. IEEE*, vol. 62, June 1974.
[6] F. F. Chen, *Plasma Physics and Controlled Fusion*. New York: Plenum Press, 1984.
[7] J. H. Richmond, "Transmission through inhomogeneous plane layers," *IRE Trans. Antennas Propagat.*, May 1962.
[8] E. F. Kuester and D. C. Chang, "Propagation, attenuation, and dispersion characteristics of inhomogeneous dielectric slab waveguides," *IEEE Trans. Microwave Theory Tech.*, vol. MTT-23, Jan. 1975.
[9] S. M. Kay and S. L. Marple, "Spectrum analysis—A modern perspective," *Proc. IEEE*, vol. 69, Nov. 1981.
[10] J. P. Rybak and R. J. Churchill, "Progress in reentry communications," *IEEE Trans. Aerospace Electron. Syst.*, vol. AES-7, Sept. 1971.
[11] R. E. Collin, *Foundations of Microwave Engineering*. New York: McGraw-Hill, 1966.
[12] R. G. Brown *et al.*, *Lines, Waves, and Antennas*. New York: Ronald Press, 1973.
[13] E. K. Miller, *Time Domain Measurements in Electromagnetics*. New York: Van Nostrand Reinhold, 1986.
[14] D. Lesselier, "Determination of index profiles by time domain reflectometry," *J. Opt.*, vol. 9, 349–358, 1978.

Gary A. Ybarra (S'83) was born in Hampton, VA, in 1960. He received the B.S. degree in 1982, the M.S. degree in 1986, and is currently pursuing the Ph.D. degree, all in electrical engineering at North Carolina State University, Raleigh.

His research interests include adaptive signal processing, digital communications, and computer modeling of radio wave propagation in nonhomogeneous plasmas.

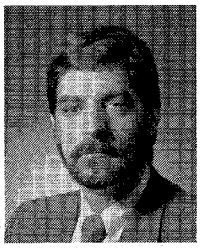

Sasan H. Ardalan (S'75–M'85) was born in Tehran, Iran, on March 20, 1956. He received the B.Sc., M.Sc., and Ph.D. degrees in electrical and computer engineering from North Carolina State University, Raleigh, in 1977, 1979, and 1983, respectively.

In August 1983 he joined the Center for Communications and Signal Processing (CCSP) at NC State as a Research Engineer. He is currently an Associate Professor of Electrical and Computer Engineering. He is the Principal Investigator of the Physical Layer in the Communications and Networking area in CCSP. He is developing research programs in computer-aided design of advanced digital communications systems, including real-time performance evaluation using multiprocessor architectures. Among his research interests are digital communications, adaptive digital signal processing, and algorithms and architectures for real-time image formation from synthetic aperture radar.

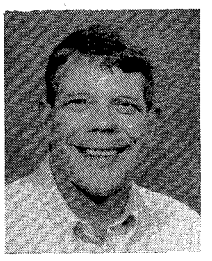

Chase P. Hearn received the B.S.E.E. degree from North Carolina State University in 1961 and the M.S.E.E. degree from the University of Virginia in 1968.

Since 1961, he has been a research engineer at the NASA Langley Research Center, where his work has involved analysis, design, and development of RF and microwave circuits and systems. His more recent work has focused on the analysis, design, and fabrication of specialized hybrid microwave integrated circuits, the application of microwave measurement and instrumentation technology to specialized materials measurements, and the development of a microwave remote ionization sensor for space technology research.

Mr. Hearn holds three patents and has one pending. He is a member of Eta Kappa Nu.

Robert E. Marshall was born in Newport News, VA. He received the B.S.E.E. and M.S.E.E. degrees from Virginia Polytechnic Institute and State University (VPI & SU) in 1971 and 1973 respectively.

After graduation he joined the Satellite Communications Group at VPI & SU, where he was involved in millimeter-wave tropospheric propagation research. In 1984 he joined the staff of the Department of Marine, Earth, and Atmospheric Sciences at North Carolina State University (NCSU), where he studied atmospheric science. In 1986 he became a visiting lecturer in the Department of Electrical and Computer Engineering at NCSU and engaged in Doppler radar meteorology research. Currently, Mr. Marshall is employed as a senior research Electrical Engineer for the Research Triangle Institute and is working as the microwave system engineer for the Microwave Reflectometer Ionization Sensor at the NASA Langley Research Center.

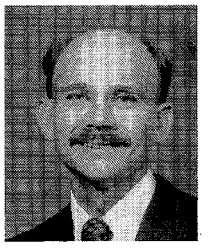

Robert T. Neece (S'82–M'86) received the Ph.D. degree in electrical engineering from North Carolina State University in 1986.

From 1986 to 1987, he was employed as a project engineer at Microwave Laboratories, Inc., in Raleigh, NC, and from 1987 to 1988, he worked as a microwave systems engineer for PRC at NASA/Langley Research Center in Hampton, VA. Since 1988, he has worked for the government at NASA/Langley as the Instrument Manager for the Microwave Reflectometer Ionization Sensor, an instrument which will be a part of NASA's Aeroassist Flight Experiment.